Journal of Sound and Vibration (2001) **241**(5), 879–893
doi:10.1006/jsvi.2000.3341, available online at http://www.idealibrary.com on IDEAL®

STABILITY AND NON-LINEAR RESPONSES OF A ROTOR–BEARING SYSTEM WITH PEDESTAL LOOSENESS

F. CHU

Department of Precision Instruments, Tsinghua University, Beijing 100084, *People's Republic of China*
E-mail: chufl@pim.tsinghua.edu.cn

AND

Y. TANG

Department of Mathematical Sciences, Tsinghua University, Beijing 100084, *People's Republic of China*

(*Received* 10 *April* 2000, *and in final form* 20 *September* 2000)

Vibration characteristics of a rotor-bearing system with pedestal looseness are investigated. A non-linear mathematical model containing stiffness and damping forces with tri-linear forms is considered. The shooting method is used to obtain the periodic solutions of the system. Stability of these periodic solutions is analyzed by using the Floquet theory. Period-doubling bifurcation and Naimark–Sacker bifurcation are found. Finally, the governing equations are integrated using the fourth order Runge–Kutta method. Different forms of periodic, quasi-periodic and chaotic vibrations are observed by taking the rotating speed and imbalance as the control parameter. Three kinds of routes to or out of chaos, that is, period-to-chaos, quasi-periodic route and intermittence, are found.

1. INTRODUCTION

In diagnosing mechanical faults of rotating machinery, it is very important to know the vibration feature of the machine with various forms of fault. A rotor system with fault is generally a complicated non-linear vibrating system. Its vibration is in a very complex form. A comprehensive investigation on periodic, quasi-periodic and chaotic vibrations of the rotating system with faults will be very beneficial to the effective fault diagnostics of rotating machinery. Pedestal looseness is one of the common faults that occur in rotating machinery. It is usually caused by the poor quality of installation or long period of vibration of the machine. Under the action of the imbalance force, the rotor system with pedestal looseness will have a periodic beating. This will generally lead to a change in stiffness of the system and the impact effect. Therefore, the system will often show very complicated vibration phenomenon.

There have been very few publications on this topic. Goldman and Muszynska [1] performed experimental, analytical and numerical investigations on the unbalance response of a rotating machine with one loose pedestal. The model was simplified as a vibrating system with bi-linear form. Synchronous and subsynchronous fractional components of the response were found. In a subsequent paper [2], they discussed the chaotic behavior of the system based on the bi-linear model.

In this paper, a simple rotor system with a disk in the middle span and with the pedestal looseness in one support is investigated theoretically. We think that the stiffness and

0022-460X/01/150879 + 15 $35.00/0

damping of the foundation to the pedestal can actually be divided into three parts while the system is vibrating. Therefore, the system is simplified as a model of differential equations with tri-linear forms of stiffness and damping. The shooting method is used to calculate the stable periodic solutions of the system. The Floquet theory is used to analyze stability and bifurcation of the periodic solutions. Finally, the equations are integrated by using the fourth order Runge–Kutta method to discuss the periodic, quasi-periodic and chaotic vibrations of the system, and the relevant phenomena. The rotating speed and imbalance are used as control parameters to investigate the bifurcation characteristics.

2. FORMULATION

The model discussed is a simple rotor system as shown in Figure 1. The rotor is supported on identical oil film bearings at both sides. The equivalent lumped mass in the position of the disk is $2m$. The shaft sections between disk and bearings are considered massless and elastic. It is assumed that the left support has pedestal looseness, the maximum static gap of the looseness is δ, and mass of the pedestal involving looseness is M. Values for the parameters of the system used in the analysis and the subsequent simulation are as follows:

$2m = 5$ kg, $c = 0{\cdot}8 \times 10^3$ Ns/m, $k = 0{\cdot}34 \times 10^6$ N/m,

$u = 0{\cdot}5 \times 10^{-4}$ m, $\delta = 0{\cdot}8$ mm, $M = 8$ kg,

$c_{f1} = 0{\cdot}2 \times 10^4$ Ns/m, $c_{f2} = 0{\cdot}2 \times 10^4$ Ns/m, $c_{f3} = 0{\cdot}2 \times 10^4$ Ns/m,

$k_{f1} = 0{\cdot}4 \times 10^8$ N/m, $k_{f2} = 0{\cdot}1 \times 10^3$ N/m, $k_{f3} = 0{\cdot}8 \times 10^6$ N/m,

$\mu = 0{\cdot}015$ Ns/m^2, $R = 50$ mm, $L = 10$ mm, $c_l = 0{\cdot}1$ mm, $g = 9{\cdot}81$ N/kg.

Based on these values the first undamped natural frequency of the rotor system is obtained as $n_1 = \sqrt{k/m} = 3521{\cdot}6$ r.p.m., or $\omega_1 = 368{\cdot}8$ 1/s.

2.1. OIL FILM FORCES OF THE BEARING

For the plain bearing, the housing is constrained from rotating. The Reynolds equation for the short-bearing approximation is given in both fixed co-ordinates [3] by

$$\frac{\partial}{\partial z}\left[\frac{h^3}{\mu}\frac{\partial p}{\partial z}\right] = 6\omega\frac{\partial h}{\partial \theta} + 12\frac{\partial h}{\partial t},$$

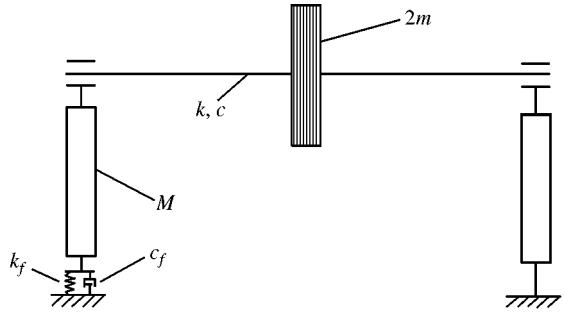

Figure 1. Schematic of the rotor-bearing system.

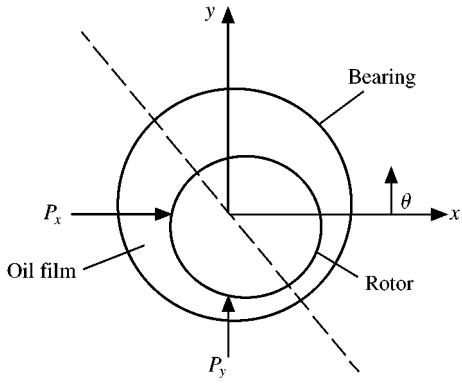

Figure 2. Schematic of the oil film bearing.

where h is the film thickness and is given by $h = c_l - x\cos\theta - y\sin\theta$, as shown in Figure 2, p is the oil film pressure, z, the axial co-ordinate, μ, the oil viscosity, ω, the rotating speed, c_l, the bearing clearance, and t, the time.

Integrating the equation for z yields

$$p(\theta, z) = \frac{3\mu}{h^3}[z^2 - Lz]\left[\omega\frac{\partial h}{\partial\theta} + 2\frac{\partial h}{\partial t}\right],$$

where L is the bearing length. The total force components in the x and y directions can be obtained by integrating the pressure over the entire journal surface as follows:

$$\begin{Bmatrix} P_x(x, y, \dot{x}, \dot{y}) \\ P_y(x, y, \dot{x}, \dot{y}) \end{Bmatrix} = \int_0^{2\pi}\int_{-L/2}^{L/2} p(\theta, z)\begin{Bmatrix}\cos\theta \\ \sin\theta\end{Bmatrix} R\,\mathrm{d}z\,\mathrm{d}\theta.$$

Finally, the two forces can be written as

$$\begin{aligned} P_x(x, y, \dot{x}, \dot{y}) &= -\mu\pi RL^3\left[\frac{\omega y + 2\dot{x}}{2(c_l^2 - x^2 - y^2)^{3/2}} + \frac{3x(x\dot{x} + y\dot{y})}{(c_l^2 - x^2 - y^2)^{5/2}}\right], \\ P_y(x, y, \dot{x}, \dot{y}) &= -\mu\pi RL^3\left[\frac{2\dot{y} - \omega x}{2(c_l^2 - x^2 - y^2)^{3/2}} + \frac{3y(x\dot{x} + y\dot{y})}{(c_l^2 - x^2 - y^2)^{5/2}}\right]. \end{aligned} \tag{1}$$

2.2. GOVERNING EQUATIONS

It is assumed that the radial displacements in the right-bearing position are x_1, y_1, in the disk position x_2, y_2, and in the left-bearing position x_3, y_3. The small movement of the left pedestal in the horizontal direction is considered negligible and its displacement in the vertical direction is assumed as y_4. The differential equations for the system can then be written as

$$c(\dot{x}_1 - \dot{x}_2) + k(x_1 - x_2) = P_{x1}(x_1, y_1, \dot{x}_1, \dot{y}_1),$$

$$c(\dot{y}_1 - \dot{y}_2) + k(y_1 - y_2) = P_{y1}(x_1, y_1, \dot{x}_1, \dot{y}_1),$$

$$
\begin{aligned}
&2m\ddot{x}_2 + c(\dot{x}_2 - \dot{x}_1) + c(\dot{x}_2 - \dot{x}_3) + k(x_2 - x_1) + k(x_2 - x_3) = 2mu\omega^2 \cos \omega t,\\
&2m\ddot{y}_2 + c(\dot{y}_2 - \dot{y}_1) + c(\dot{y}_2 - \dot{y}_3) + k(y_2 - y_1) + k(y_2 - y_3) = 2mu\omega^2 \sin \omega t - 2mg,\\
&c(\dot{x}_3 - \dot{x}_2) + k(x_3 - x_2) = P_{x3}(x_3, y_3 - y_4, \dot{x}_3, \dot{y}_3 - \dot{y}_4),\\
&c(\dot{y}_3 - \dot{y}_2) + k(y_3 - y_2) = P_{y3}(x_3, y_3 - y_4, \dot{x}_3, \dot{y}_3 - \dot{y}_4),\\
&M\ddot{y}_4 + c_f\dot{y}_4 + k_f y_4 = -P_{y3}(x_3, y_3 - y_4, \dot{x}_3, \dot{y}_3 - \dot{y}_4) - Mg,
\end{aligned}
\tag{2}
$$

where the change in the unbalance of the rotating disk and shaft caused by the looseness gap is neglected. In the above equation c is the damping coefficient of shaft, k the stiffness coefficient, u the unbalance, P_{x1}, P_{y1} the oil film force components of the right bearing in the x and y directions, P_{x3}, P_{y3} of the left bearing, and c_f, k_f are the damping and stiffness coefficients of the foundation or the joint to the pedestal. When the looseness occurs, these two coefficients can be expressed by

$$
c_f = \begin{cases} c_{f1}, & y_4 < 0, \\ c_{f2}, & 0 \leqslant y_4 \leqslant \delta, \\ c_{f3}, & y_4 > \delta, \end{cases}
\qquad
k_f = \begin{cases} k_{f1}, & y_4 < 0, \\ k_{f2}, & 0 \leqslant y_4 \leqslant \delta, \\ k_{f2} + k_{f3} - k_{f3}\dfrac{\delta}{y_4}, & y_4 > \delta, \end{cases}
\tag{3}
$$

where the stiffness and damping actions are considered in three parts. When $y_4 = 0$, the pedestal is in contact with the foundation. $y_4 < 0$ means that the pedestal and the foundation are in compression state and the impact is considered elastic. $y_4 > \delta$ describes the extension of the joint and also the deformation of the joint is assumed as elastic. Equation (2) including equation (3) is a non-linear vibrating system with piecewise-linear stiffness and damping.

If one assumes that

$$
\omega t = \tau, \qquad \frac{\mathrm{d}}{\mathrm{d}\tau} = {}',
$$

$$
\begin{gathered}
x_1 = s_1, \quad y_1 = s_2, \quad x_2 = s_3, \quad x_2{}' = s_4, \quad y_2 = s_5, \quad y_2{}' = s_6,\\
x_3 = s_7, \quad y_3 = s_8, \quad y_4 = s_9, \quad y_4{}' = s_{10}
\end{gathered}
\tag{4}
$$

and

$$
\begin{gathered}
D_1 = \pi\mu RL^3, \quad D_2 = (c_l^2 - x_1^2 - y_1^2)^{3/2}, \quad D_3 = (c_l^2 - x_1^2 - y_1^2)^{5/2},\\
D_4 = [c_l^2 - x_3^2 - (y_3 - y_4)^2]^{3/2}, \qquad D_5 = [c_l^2 - x_3^2 - (y_3 - y_4)^2]^{5/2},
\end{gathered}
\tag{5}
$$

then equation (2) can be transferred into a set of first order differential equations in the form of $S' = f(S, S', \tau)$ as

$$
s_1' = (D_8D_9 - D_7D_{10})/(D_6D_9 - D_7D_7), \qquad s_2' = (D_6D_{10} - D_7D_8)/(D_6D_9 - D_7D_7),
$$

$$
s_3' = s_4, \qquad s_4' = \frac{1}{2m\omega^2}[-c\omega(2s_4 - s_1' - s_7') - k(2s_3 - s_1 - s_7)] + u\cos\tau,
$$

$$s'_5 = s_6, \qquad s'_6 = \frac{1}{2m\omega^2}\left[-c\omega(2s_6 - s'_2 - s'_8) - k(2s_5 - s_2 - s_8)\right] + u\sin\tau - \frac{g}{\omega^2},$$

$$s'_7 = (D_{13}D_{14} - D_{12}D_{15})/(D_{11}D_{14} - D_{12}D_{12}), \tag{6}$$

$$s'_8 = (D_{11}D_{15} - D_{12}D_{13})/(D_{11}D_{14} - D_{12}D_{12}), \qquad s'_9 = s_{10},$$

$$s'_{10} = -\frac{1}{M\omega^2}(c_f\omega s_{10} + k_f s_9) - \frac{D_1}{2D_4D_5M\omega^2}\{D_5\omega(2s'_8 - 2s_{10} - s_7)$$

$$+ 6D_4\omega(s_8 - s_9)[s_7s'_7 + (s_8 - s_9)(s'_8 - s_{10})]\} - \frac{g}{\omega^2},$$

where

$$D_6 = 2D_2D_3c\omega + 2D_1D_3\omega + 6D_1D_2\omega s_1^2, \qquad D_7 = 6D_1D_2\omega s_1 s_2,$$

$$D_8 = 2D_2D_3c\omega s_4 - 2D_2D_3k(s_1 - s_3) - D_1D_3\omega s_2,$$

$$D_9 = 2D_2D_3c\omega + 2D_1D_3\omega + 6D_1D_2\omega s_2^2,$$

$$D_{10} = 2D_2D_3c\omega s_6 - 2D_2D_3k(s_2 - s_5) + D_1D_3\omega s_1,$$

$$D_{11} = 2D_4D_5c\omega + 2D_1D_5\omega + 6D_1D_4\omega s_7^2, \qquad D_{12} = 6D_1D_4\omega s_7(s_8 - s_9),$$

$$D_{13} = 2D_4D_5(c\omega s_4 - ks_7 + ks_3) - D_1D_5\omega(s_8 - s_9) + 6D_1D_4\omega s_7(s_8 - s_9)s_{10},$$

$$D_{14} = 2D_4D_5c\omega + 2D_1D_5\omega + 6D_1D_4\omega(s_8 - s_9)^2,$$

$$D_{15} = 2D_4D_5(c\omega s_6 - ks_8 + ks_5) + D_1D_5\omega(2s_{10} + s_7) + 6D_1D_4\omega(s_8 - s_9)^2 s_{10}.$$

In equation (6), some of the right-hand terms contain derivatives. In performing numerical integration, one can compute s'_1, s'_2, s'_7, s'_8 first, then use the obtained results to calculate other derivatives. In this way, the problem $S' = f(S', S, \tau)$ can be processed by using the same method as in the form of $S' = g(S, \tau)$.

3. BIFURCATION AND STABILITY ANALYSIS

Equation (6) is a non-linear vibrating system with seven degrees of freedom and with piecewise-linear form. Because of these features, when performing a theoretically qualitative analysis it is very difficult to discuss the equations of motion in an analytical way and impossible to obtain the solutions in a closed form. Therefore, numerical methods have to be resorted.

There have been several methods for determining the periodic response of the non-linear rotor systems, including the series expansion [4] and the harmonic balance method as used in references [5, 6]. However, for a multi-degree of freedom, these methods often suffer the problem of convergence to some extent when iteration is performed. In this aspect, the shooting method has shown good ability of convergence. The shooting method has been previously used to obtain periodic solutions of non-linear differential equations. The

algorithm is based on the utilization of the Poincare's map in which the flow of an nth order continuous-time system is replaced with an $(n-1)$th order discrete-time system, thus transforming the problem of finding a periodic solution to that of finding a fixed point. Kaas–Petersen [7] discussed the method and extended it to find quasi-periodic solutions. In this section, the shooting method to calculate periodic solutions and to analyze stability is presented followed by some of the numerical results.

Consider a system described by the following equation:

$$\dot{s} = f(s, \omega, t) \in R^n, \tag{7}$$

where f is periodic in t with period $T = 2\pi/\omega$, $f(s, \omega, t + T) = f(s, \omega, t)$ and $s = (s_1, s_2, \ldots, s_n) \in R^n$. For $s^0 \in R^n$, let $q(t, s^0)$ be the solution of equation (7) with initial value $g(0, s^0) = s^0$. Then the Poincare's map for the system (7) is

$$P : R^n \to R^n, \qquad P(s) = q(T, s). \tag{8}$$

A T-periodic orbit $q(t, s^0)$ of equation (7) obviously corresponds to a fixed point of the Poincare's map (8), $P(s^0) = s^0$.

The map P can be used to define a map Q as follows:

$$Q = P - I, \tag{9}$$

where I is the identity. Then a periodic solution of equation (7) corresponds to a zero of Q. Newton–Raphson method is very efficient for the purpose of finding zeros of Q. The values of Q(s) and the derivative DQ(s) needed for the iteration procedure can be computed numerically. The iteration formula can then be obtained as

$$s^{k+1} = s^k - [DQ(s^k)]^{-1} Q(s^k), \qquad k = 0, 1, \ldots . \tag{10}$$

The iteration process is repeated until $\| Q(s^k) \| < \varepsilon$ for some preassigned ε. If too many iterations are performed, then the process is stopped, which could be an indication of a too poor initial guess. The convergent result of $\{s^k\}$ as a fixed point of the map P is just a periodic solution to the system (7).

For the stability analysis, based on the iteration result, stability of a periodic solution could be determined as the stability of the fixed point. Now let s be the fixed point of the map P, so

$$s = P(s).$$

If εu is any disturbance, then by Taylor's theorem

$$P(s + \varepsilon u) = P(s) + DP(s)\varepsilon u + O(|\varepsilon|^2).$$

Let $s + \varepsilon u$ be mapped into $s + \phi$, then

$$s + \phi = P(s + \varepsilon u) = P(s) + DP(s)\varepsilon u + O(|\varepsilon|^2).$$

Retaining only the lowest-order terms gives

$$\phi = DP(s)\varepsilon u. \tag{11}$$

s is stable when any disturbance εu yields a ϕ such that $\|\phi\| < |\varepsilon|$. This is fulfilled if all eigenvalues of $DP(s)$ are inside the unit circle. Since $Q = P - I$, DP can be obtained by

$$DP(s) = DQ(s) + I. \tag{12}$$

The eigenvalues of $DP(s)$ are the Floquet multipliers [8], or the characteristic multipliers. Therefore, it is possible to use Floquet theory to discuss the stability of the periodic solution. If the Floquet multipliers of the system are $\lambda_1, \lambda_2, \ldots, \lambda_{10}$, concerning bifurcation and stability of equation (6), there are the following conclusions:

(1) When $|\lambda_i| < 1$ ($i = 1, 2, \ldots, n$ and $n_s = \infty$), the stable periodic solution of equation (6) is asymptotically stable.

(2) If there is one λ_j which passes the unit circle outwards through the point of -1 and other $|\lambda_i|_{i \neq j} < 1$ ($i = 1, 2, \ldots, n$), the stable periodic solution will have the period-doubling bifurcation.

(3) If there is one λ_j which passes the unit circle outwards through the point of $+1$ and other $|\lambda_i|_{i \neq j} < 1$ ($i = 1, 2, \ldots, n$), the stable periodic solution will have the saddle-node bifurcation.

(4) If there is a pair of conjugate complex characteristic multipliers $\lambda_j = a \pm ib$ which pass the unit circle outwards and other $|\lambda_i|_{i \neq j} < 1$ ($i = 1, 2, \ldots, n$), the stable periodic solution will have the Naimark–Sacker bifurcation [9] and the bifurcation will lead to an invariant torus.

The above-discussed shooting method is used to obtain the periodic solutions of equation (6) for some rotating speeds. The Floquet multipliers at different rotating speeds are obtained as shown in Table 1. It can be seen that at some rotating speeds, the system will

TABLE 1

Characteristics of the rotor system at different rotating speeds

ω/ω_1	Floquet multipliers λ_1	Conclusions
0·64	− 1·08279 + i0·0; − 1·03667 + i0·0 − 0·65323 + i0·12867; − 0·65323 − i0·12867 − 0·11665 + i0·06240; − 0·11665 − i0·06240 0·01217 + i0·0; − 0·01101 + i0·0 − 0·01047 + i0·00732; − 0·01047 − i0·00732	Period-doubling bifurcation
1·98	− 1·28657 + i0·36588; − 1·28657 − i0·36588 − 0·67434 + i0·06945; − 0·67434 − i0·06945 − 0·14346 + i0·19808; − 0·14346 − i0·19808 − 0·41499 + i0·21141; − 0·41499 − i0·21141 − 0·21215 + i0·06682; − 0·21215 − i0·06682	Naimark–Sacker bifurcation
2·83	− 1·02718 + i0·60448; − 1·02718 − i0·60448 − 0·72867 + i0·19399; − 0·72867 − i0·19399 − 0·23703 + i0·49386; − 0·23703 − i0·49386 0·01937 + i0·37864; 0·01937 − i0·37864 − 0·16616 + i0·30358; − 0·16616 − i0·30358	Naimark–Sacker bifurcation
6·22	− 0·77510 + i0·54037; − 0·77510 − i0·54037 − 0·71783 + i0·39661; − 0·71783 − i0·39661 0·47102 + i0·65186; 0·47102 − i0·65186 0·49991 + i0·40466; 0·49991 − i0·40466 0·38520 + i0·51588; 0·38520 − i0·51588	Periodic solution is stable

become unstable and exhibit Naimark–Sacker bifurcation. Also, as appeared in the bi-linear oscillator [10, 11], this tri-linear oscillator has period-doubling bifurcation as well.

4. NUMERICAL SIMULATION

The shooting method is to some extent still an approximate method for analyzing a non-linear system. In order to further observe the dynamic behavior of the system, the fourth order Runge–Kutta method was then used to integrate equation (6). In this section, the rotating speed and imbalance were used as the control parameters to perform a detailed investigation on bifurcation, chaos, and the routes to or out of chaos.

During integration, a smaller marching step is chosen to ensure a stable solution and to avoid the numeric divergence at the point where damping and stiffness coefficients are discontinuous. Generally, long time-marching computation is needed to obtain a convergent orbit. In the case of a strongly stable motion with heavy damping, several hundred periods of integration may be enough while for some other cases several thousand periods are necessary.

To illustrate the motion behavior of the system, the orbit, the Poincare's map and the bifurcation diagram are used. A Poincare's section is a stroboscopic picture of a motion and consists of the time series at a constant interval of T with T being the period of excitation. The corresponding Poincare's map is a combination of those return points and after iterating enough times these points may converge at a subset which is often called an attractor. Examination of the distribution of return points on the Poincare's map can reveal the nature of motion. In the case of a periodic motion, the N discrete points on the Poincare's map indicate that the period of motion is NT. In the case of a quasi-periodic motion, return points appear to fill up a closed curve in the Poincare's map. For a chaotic motion, return points form a geometrically fractal structure. The bifurcation diagram is another type of plot to reflect the motion change. To compute a bifurcation diagram, a control parameter was varied at a constant step. The variation of the Y (y_2/c_l) co-ordinate of the return point in the Poincare's map versus the control parameter to form a bifurcation diagram was then plotted. In this paper, the motion of the disk position in the form of x_2/c_l and y_2/c_l was recorded to form orbits and the corresponding Poincare's maps and bifurcation diagrams. In some cases, the orbits at the left-bearing position in the form of x_3/c_l and y_3/c_l were also presented.

In order to judge whether a motion is chaotic or not, a method discussed by Wolf *et al.* [12] was used to calculate the maximum Lyapunov exponent. The program contained in reference [12] for ordinary differential equations plus the IMSL-routine DVERK was used to perform this calculation. Also to describe the fractal behavior of the attractor quantitatively the information dimension was calculated for some cases. The information dimension is one of the many definitions of the fractal dimension that measures the extent to which the points fill a subspace as the number of points becomes large [13].

It has to be pointed out that in figures presented in this paper the same amount of data of 80 periods are used in all orbit plots but with different scales and also the different scales are used in the Poincare's maps in order to amplify the attractors and to reflect the shape of an attractor adequately.

Figure 3 is the bifurcation diagram of the system by using the rotating speed as the control parameter where for every rotating speed 100 points are included. It can be seen that at very low rotating speeds the motion is synchronous with period-2. The bifurcation map shows two points for every rotating speed. But by examining the Poincare's map carefully it is found that the motion is actually quasi-periodic and the Poincare's return points move

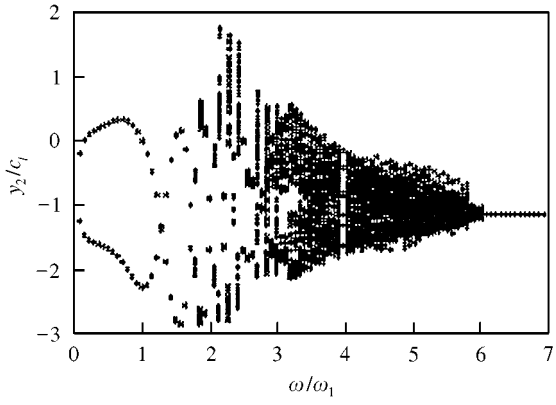

Figure 3. Bifurcation diagram by using ω/ω_1 as the control parameter showing the dynamic characteristic in the process of increasing speed.

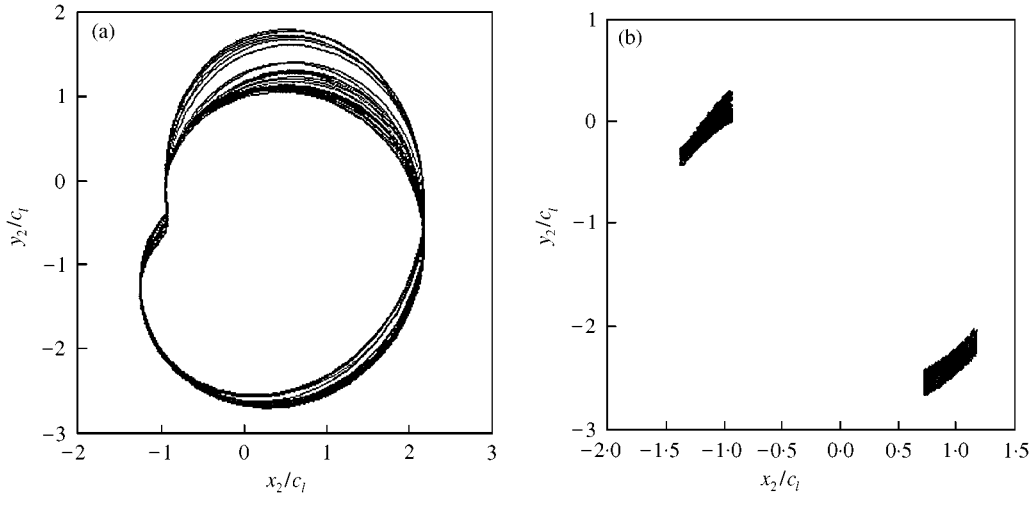

Figure 4. Orbit (a) and Poincare's map (b) at disk position for $\omega/\omega_1 = 1{\cdot}77$.

very slowly. It is difficult to see the return points to form a closed curve because the data amount is too large. As the rotating speed increases further the attractor diverges and at about $\omega/\omega_1 = 1{\cdot}70$ the motion becomes chaotic. An example of the chaotic picture, in the form of orbit and Poincare's map, is shown in Figure 4, where $\omega/\omega_1 = 1{\cdot}77$. The Poincare's map was obtained by recording data from period 2001 to period 10,000 and the maximum Lyapunov exponent was computed to be 3·08. Figure 5 is the orbit and Poincare's map for $\omega/\omega_1 = 3{\cdot}54$. The attractor is a clear indication of chaotic motion in which stretching and folding can be clearly seen and the information dimension was calculated to be 1·21. In order to see if there is any rub happening between the rotor and the left bearing, the orbit at the left-bearing position is also shown in Figure 5. The chaotic motion remains until $\omega/\omega_1 = 6{\cdot}06209$ and at $\omega/\omega_1 = 6{\cdot}06210$ the motion suddenly becomes periodic. Figure 6 shows two orbits at the disk position and the left-bearing position for $\omega/\omega_1 = 5{\cdot}66$. Figure 7 is the Poincares map and the orbit at the disk position and the orbit at the left-bearing position for $\omega/\omega_1 = 6{\cdot}06$. An interesting phenomenon that can be seen is that the disk is

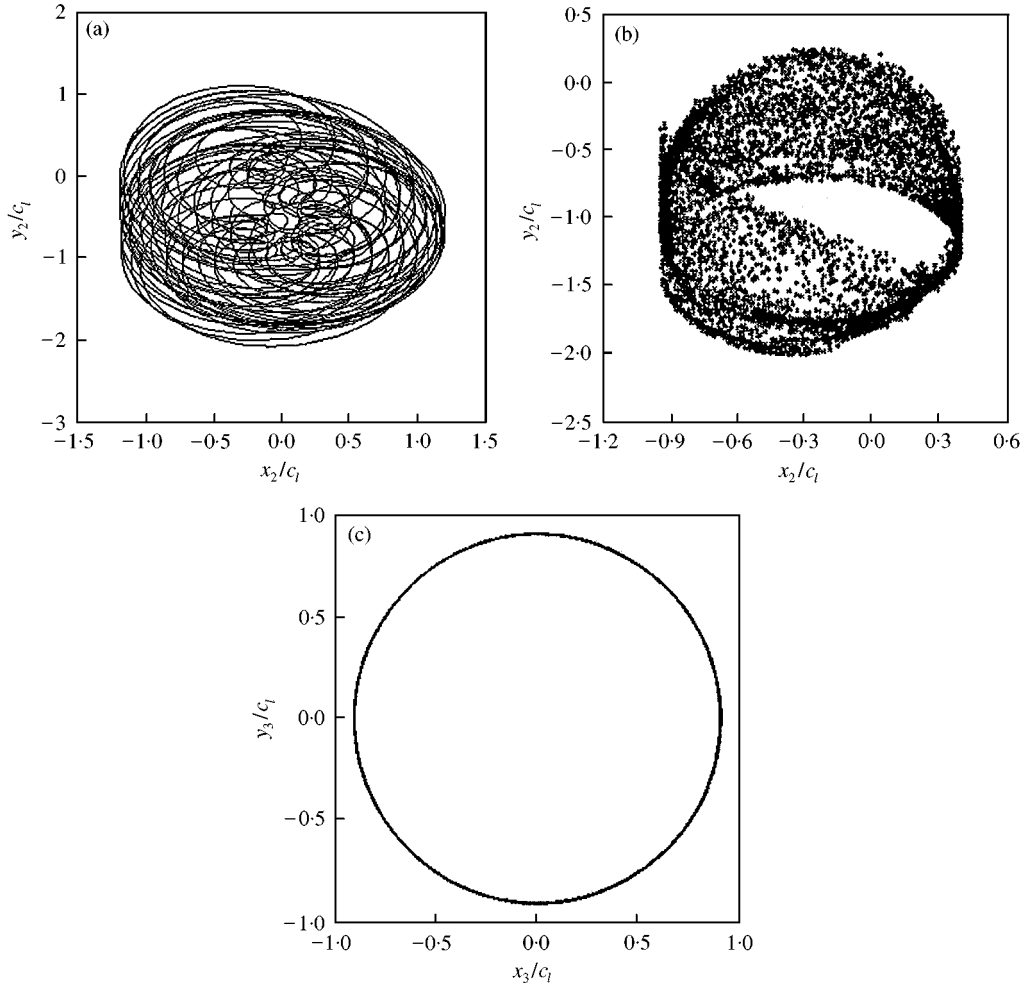

Figure 5. Orbit (a) and Poincare's map (b) at disk position and orbit (c) at left-bearing position for $\omega/\omega_1 = 3{\cdot}54$.

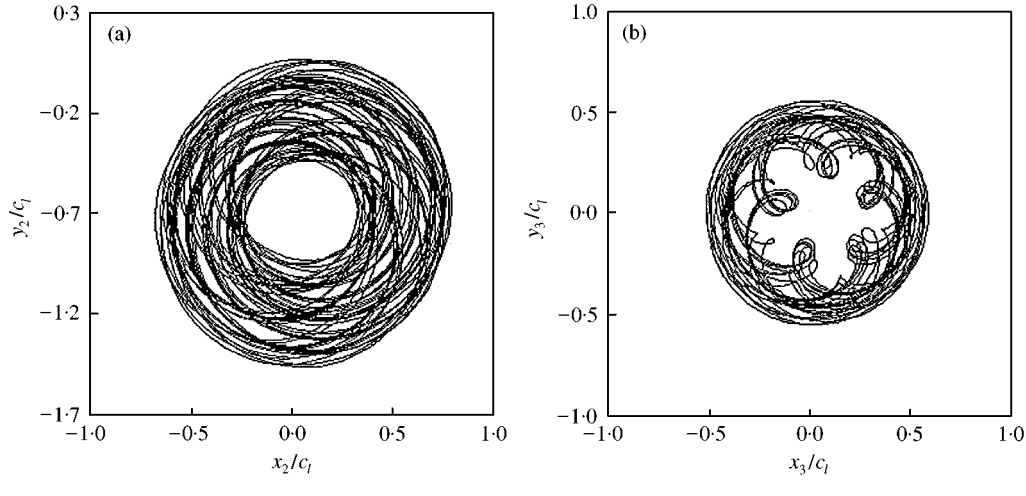

Figure 6. Orbits at disk position (a) and at left-bearing position (b) for $\omega/\omega_1 = 5{\cdot}66$.

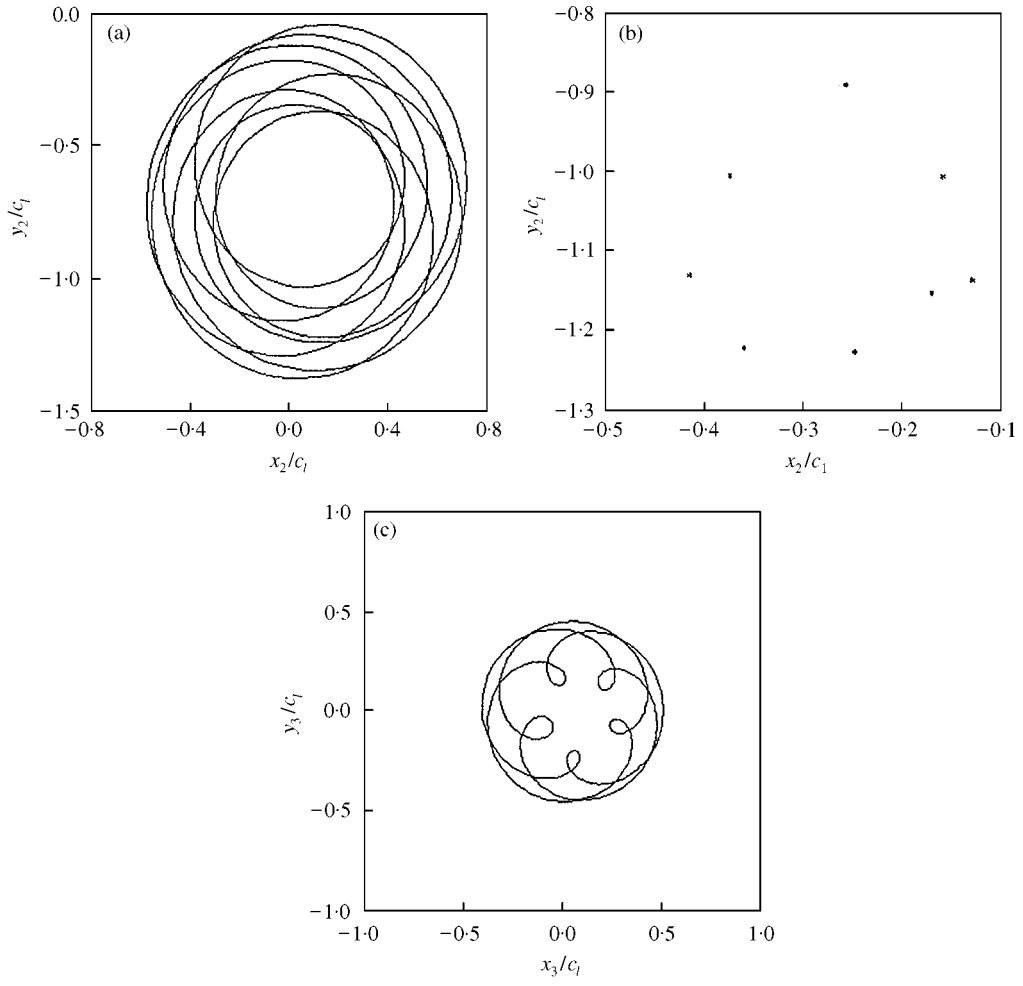

Figure 7. Orbit (a) and Poincare's map (b) at disk position and orbit (c) at left-bearing position for $\omega/\omega_1 = 6{\cdot}06$.

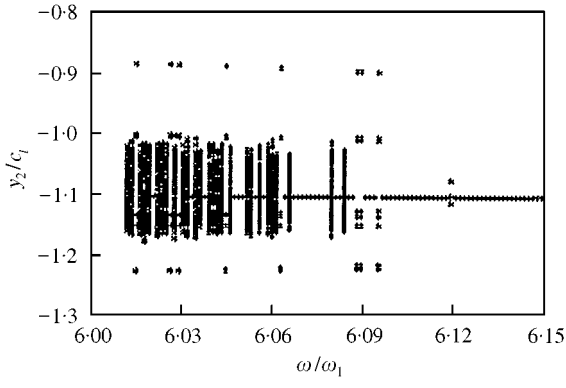

Figure 8. Bifurcation diagram by using ω/ω_1 as the control parameter showing the route of intermittence.

vibrating in the form of period-8 but the left end of the rotor is in period-5. Finally, the motion was found to leave the chaotic region in a route of intermittence as shown in Figure 8, where chaotic motion and periodic vibration alternates in a range of rotating

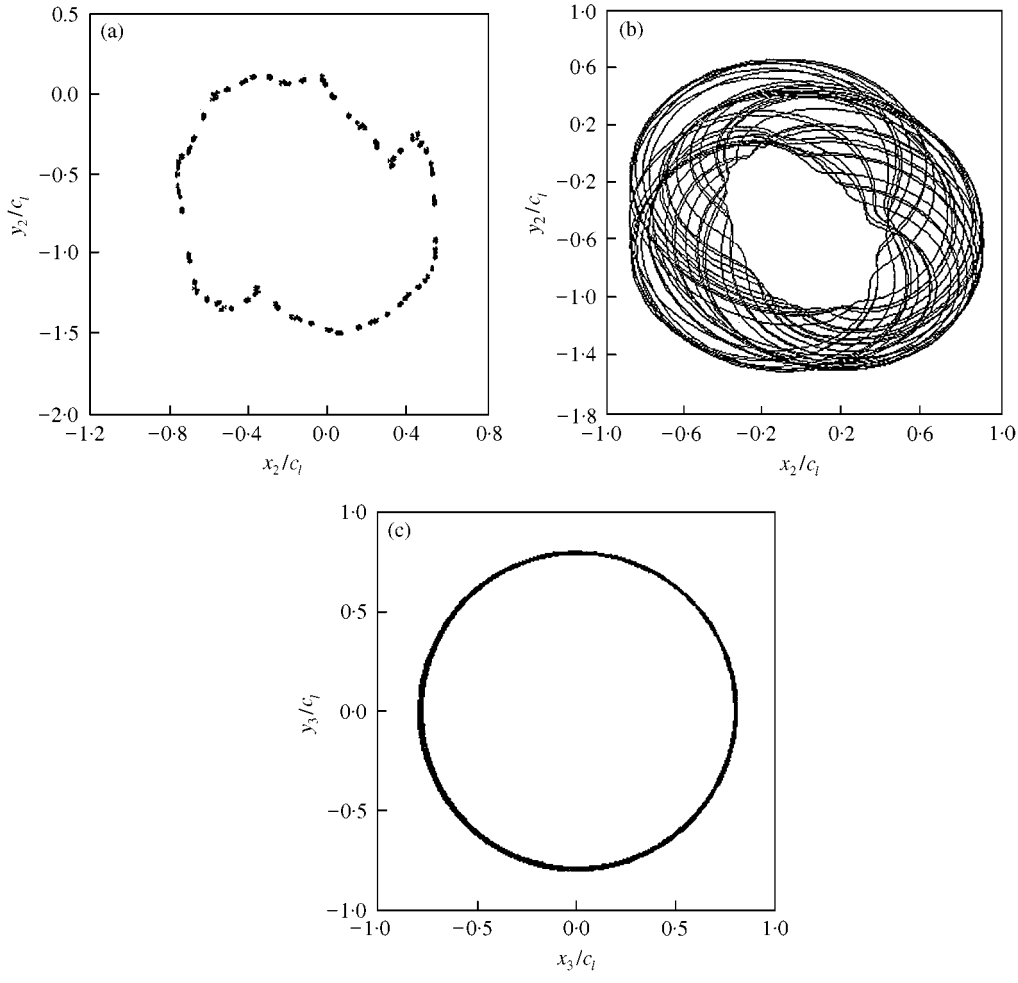

Figure 9. Poincare's map (a) and orbit (b) at disk position and orbit (c) at left-bearing position for $u = 0{\cdot}0220947498313$ mm.

speed and the motion settles into periodic finally. This is different from the route of intermittence found in the rub-impact system [10]. In conclusion, when the rotating speed is used as the control parameter the motion enters into the chaotic region in the quasi-periodic route and leaves in a route of intermittence.

We now take imbalance as the control parameter to see various forms of vibration and the route to or out of chaos. In this case, we fix $\omega/\omega_1 = 3{\cdot}54$. Figure 9 is the Poincare's map at the disk position, and orbits at both the disk position and the left-bearing position for $u = 0{\cdot}0220947498313$ mm and the motion can be found periodic. Figure 10 is for $u = 0{\cdot}0220947498314$ mm and the motion becomes chaotic. The maximum Lyapunov exponent was calculated as 0·3302 in this case. It can be seen that the route to chaos is a kind of period-to-chaos, or crisis, a route mentioned recently in several publications [10, 14]. If we further increase the imbalance, various forms of chaotic vibrations can be found. Figure 11 is the Poincare's map and the orbit at the disk position where $u = 0{\cdot}1699999999$ mm. The attractor is very loose and the information dimension was calculated to be 1·38. Figure 12 is for $u = 0{\cdot}17$ mm where the motion has become

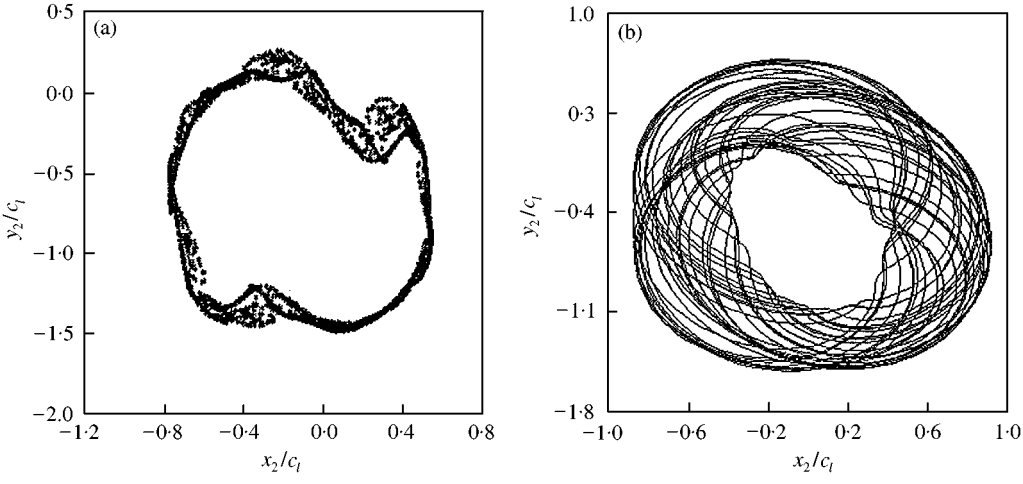

Figure 10. Poincare's map (a) and orbit (b) at disk position for $u = 0{\cdot}0220947498314$ mm.

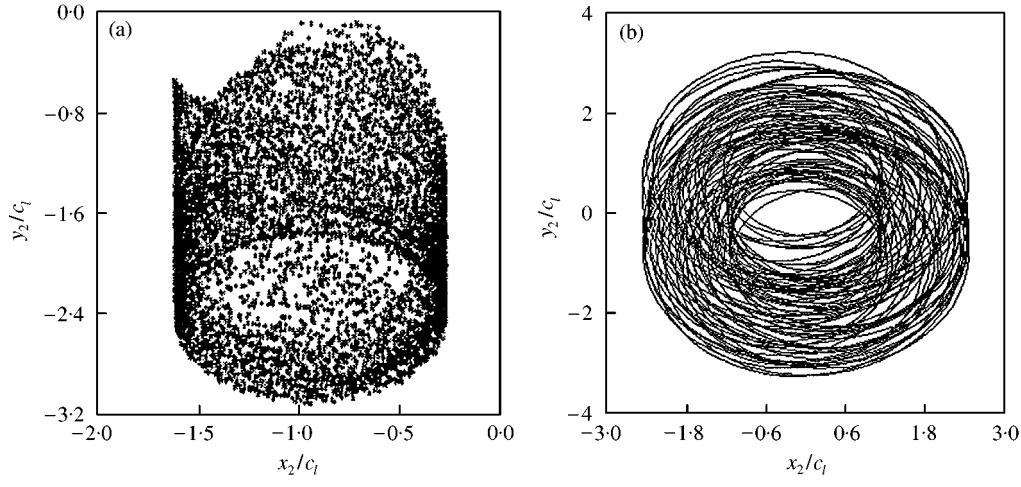

Figure 11. Poincare's map (a) and orbit (b) at disk position for $u = 0{\cdot}1699999999$ mm.

quasi-periodic. Therefore, the route out of chaos in this case is quasi-periodic. In conclusion, when imbalance is used as the control parameter the motion enters into the chaotic region in the period-to-chaos route and leaves the region in the quasi-periodic route.

5. CONCLUSIONS

A mathematical model of the rotor-bearing system with pedestal looseness is presented. The model is a non-linear vibrating system containing piece-wise damping and stiffness forces with the tri-linear forms. A shooting method is used to calculate the stable periodic solutions of the system and the method is found very efficient. The Floquet theory is used to analyze stability and bifurcation of the periodic solutions. Period-doubling bifurcation and Naimark–Sacker bifurcation are found.

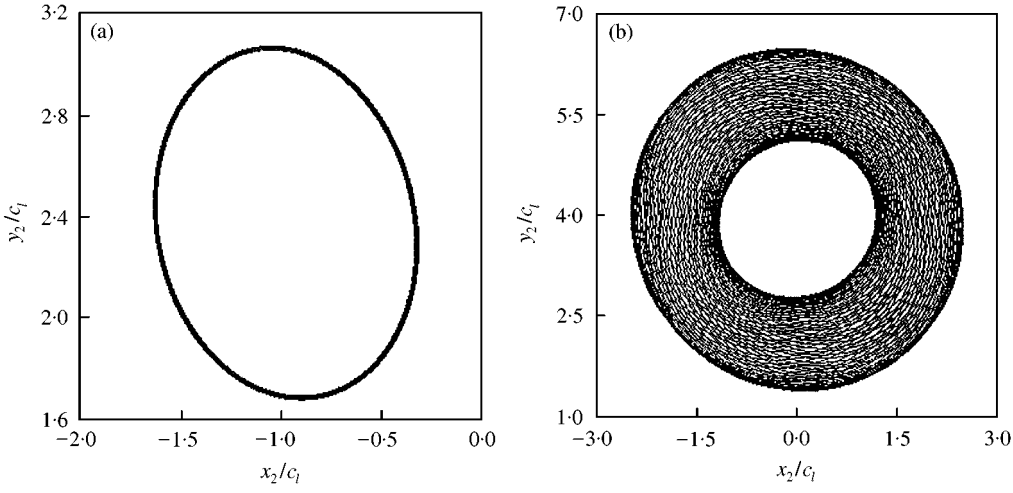

Figure 12. Poincare's map (a) and orbit (b) at disk position for $u = 0{\cdot}17$ mm.

The fourth order Runge–Kutta method is used to integrate the governing equations. Very rich forms of periodic, quasi-periodic and chaotic vibrations can be observed. Three types of route to or out of chaos, that is, period-to-chaos, quasi-periodic route and intermittence, are found. The analytical results are very important for diagnosing the pedestal looseness in rotating machinery.

ACKNOWLEDGMENTS

This research is supported financially by a project from the Ministry of Science and Technology in China (Grant No. PD9521908Z2), National Natural Science Foundation of China (Grant No. 19990510) and Tsinghua University Basic Research Foundation (Grant No. Jc1999045).

REFERENCES

1. P. GOLDMAN and A. MUSZYNSKA 1991 *Rotating Machinery and Vehicle Dynamics, American Society of Mechanical Engineers DE-Vol.* **35**, 11–17. Analytical and experimental simulation of loose pedestal dynamic effects on a rotating machine vibrational response.
2. A. MUSZYNSKA and P. GOLDMAN 1995 *Chaos Solitons & Fractals* **5**, 1683–1704. Chaotic responses of unbalanced rotor-bearing stator systems with looseness or rubs.
3. E. J. GUNTER, L. E. BARRETT and P. E. ALLAIRE 1977 *Journal of Lubrication Technology, Transactions of the American Society of Mechanical Engineers* **99**, 57–64. Design of nonlinear squeeze-film dampers for aircraft engines.
4. F. CHU and Z. ZHANG 1998 *Journal of Sound and Vibration* **210**, 1–18. Bifurcation and chaos in a rub-impact Jeffcott rotor system
5. Y. B. KIM and S. T. NOAH 1991 *Journal of Applied Mechanics, Transactions of the American Society of Mechanical Engineers* **58**, 545–553. Stability and bifurcation analysis of oscillators with piecewise-linear characteristics: a general approach.
6. F. CHU and R. HOLMES 1998 *Computer Methods in Applied Mechanics and Engineering* **164**, 363–373. Efficient computation on nonlinear responses of a rotating assembly incorporating the squeeze-film damper.
7. C. KAAS-PETERSEN 1985 *Journal of Computational Physics* **58**, 395–408. Computation of quasi-periodic solutions of forced dissipative systems.

8. S. K. CHOI and S. T. NOAH 1992 *Nonlinear Dynamics* **3**, 105–121. Response and stability analysis of piecewise-linear oscillators under multi-forcing frequencies.
9. S. WIGGINS 1990 *Introduction to Applied Nonlinear Dynamical Systems and Chaos*. New York: Springer-Verlag.
10. F. CHU and Z. ZHANG 1997 *International Journal of Engineering Science* **35**, 963–973. Periodic, quasi-periodic and chaotic vibrations of a rub-impact rotor system supported on oil film bearings.
11. J. M. T. THOMPSON and H. B. STEWART 1986 *Nonlinear Dynamics and Chaos, Geometrical Methods for Engineers and Scientists*. Chichester: John Wiley.
12. A. WOLF, J. B. SWIFT, H. L. SWINNEY and J. A. VASTANO 1985 *Physica D* **16**, 285–317. Determining Lyapunov exponents from a time-series.
13. F. C. MOON 1988 *Chaotic Vibrations*. New York: John Wiley & Sons.
14. G. SUIRE and G. CEDERBAUM 1995 *International Journal of Mechanical Sciences* **37**, 753–772. Periodic and chaotic behavior of viscoelastic nonlinear (elastica) bars under harmonic excitations.